NUMERICAL TIME DOMAIN MODELING OF PIEZOELECTRIC TRANSDUCERS/ SENSORS AND ULTRASONIC WAVE PHENOMENA WITH THE PIEZOELECTRIC FINITE INTEGRATION TECHNIQUE (PFIT)

R. Marklein, O. Glitza, T. Kaczorowski, K.–J. Langenberg
Department of Electrical Engineering
University of Kassel
D–34109 Kassel, Germany

INTRODUCTION

Today, the applications of piezoelectric materials in transducers/sensors are widespread, e. g., in pulse–echo systems in nondestructive testing (NDT) or medical imaging (sonography) with ultrasound. The goal of this work is to derive a numerical modeling tool for the development and optimization of piezoelectric transducers/sensors, and/or to get a deeper understanding of the wave propagation in piezoelectric materials applying computer simulations [1,2]. The piezoelectric effect is a linear effect and couples the governing equations of electromagnetics and elastodynamics [3,4].

This paper presents a novel numerical method, the Piezoelectric Finite Integration Technique (PFIT), to model piezoelectric transducers/sensors and ultrasonic wave phenomena in the time domain [5]. PFIT is derived within the electroquasistatic (EQS) approximation from the governing equations in integral form by applying the well–established Finite Integration Technique (FIT). Voltage/charge driven and current driven PFIT algorithms have been developed, called U–PFIT and I–PFIT, respectively. In order to model the excitation mode as well as the reception mode of a piezoelectric transducer by a voltage generator including the internal resistance R_{g} of the voltage generator in the numerical modeling scheme the I–PFIT algorithm is combined with a network algorithm. The resulting algorithm is here checked against measurements and results of a 1–D lattice model [6]. Further results can be found in [5].

LINEAR PIEZOELECTRICITY AND THE PIEZOELECTRIC FINITE INTEGRATION TECHNIQUE

For a linear, inhomogeneous, dissipative (viscid), piezoelectric material the constitutive equations are

$$\begin{aligned}
\underline{\mathbf{j}}(\underline{\mathbf{R}},t) &= \rho_{\mathrm{p0}}(\underline{\mathbf{R}})\,\underline{\mathbf{v}}(\underline{\mathbf{R}},t)\\
\underline{\mathbf{D}}(\underline{\mathbf{R}},t) &= \underline{\underline{\boldsymbol{\varepsilon}}}^{\mathrm{S}}(\underline{\mathbf{R}})\cdot\underline{\mathbf{E}}(\underline{\mathbf{R}},t) + \underline{\underline{\underline{\mathbf{e}}}}(\underline{\mathbf{R}}):\underline{\underline{\mathbf{S}}}(\underline{\mathbf{R}},t)\\
\underline{\underline{\mathbf{S}}}(\underline{\mathbf{R}},t) &= \underline{\underline{\underline{\underline{\mathbf{s}}}}}^{\mathrm{E}}(\underline{\mathbf{R}}):\underline{\underline{\mathbf{T}}}(\underline{\mathbf{R}},t) - \underline{\underline{\underline{\underline{\boldsymbol{\tau}}}}}^{\mathrm{E}}(\underline{\mathbf{R}}):\underline{\underline{\mathbf{D}}}(\underline{\mathbf{R}},t) + \underline{\underline{\underline{\underline{\mathbf{d}}}}}^{231}(\underline{\mathbf{R}})\cdot\underline{\mathbf{E}}(\underline{\mathbf{R}},t)
\end{aligned}$$

with the linear momentum density vector $\underline{\mathbf{j}}$, position vector $\underline{\mathbf{R}}$, time t, mass density at rest ρ_{p0}, particle velocity vector $\underline{\mathbf{v}}$, electric flux density vector $\underline{\mathbf{D}}$, permittivity tensor $\underline{\underline{\boldsymbol{\varepsilon}}}^{\mathrm{S}}$, electric field strength vector $\underline{\mathbf{E}}$, piezoelectric coupling tensor $\underline{\underline{\mathbf{e}}}$, deformation tensor $\underline{\underline{\mathbf{S}}}$, compliance tensor $\underline{\underline{\underline{\mathbf{s}}}}^{\mathrm{E}}$, Cauchy stress tensor $\underline{\underline{\mathbf{T}}}$, relaxation tensor $\underline{\underline{\underline{\boldsymbol{\tau}}}}^{\mathrm{E}}$, symmetric velocity gradient tensor $\underline{\underline{\mathbf{D}}} = \mathrm{sym}\{\boldsymbol{\nabla}\underline{\mathbf{v}}\}$, and the piezoelectric coupling tensor $\underline{\underline{\underline{\mathbf{d}}}}$. All field quantities are functions of the position vector $\underline{\mathbf{R}} = x_i\underline{\mathbf{e}}_i$ (summation convention) and time t, and all material properties are functions of $\underline{\mathbf{R}}$ only. The centered dot represents the scalar product and the colon denotes the double–scalar product with the property $\underline{\mathbf{a}}\,\underline{\mathbf{b}} : \underline{\mathbf{c}}\,\underline{\mathbf{d}} = (\underline{\mathbf{a}}\cdot\underline{\mathbf{d}})(\underline{\mathbf{b}}\cdot\underline{\mathbf{c}})$. The upper indicial notation 231 indicates transposition of the tensor elements: $\underline{\underline{\underline{\mathbf{d}}}}^{231} = (\mathrm{d}_{ijk}\underline{\mathbf{e}}_i\underline{\mathbf{e}}_j\underline{\mathbf{e}}_k)^{231} = \mathrm{d}_{ijk}\underline{\mathbf{e}}_j\underline{\mathbf{e}}_k\underline{\mathbf{e}}_i$.

If the dimension of the piezoelectric material is small compared to the electromagnetic wavelength, it is convenient to introduce the electroquasistatic (EQS) approximation $\underline{\mathbf{E}}(\underline{\mathbf{R}},t) = -\boldsymbol{\nabla}\Phi(\underline{\mathbf{R}},t)$ with the electric scalar potential Φ [e. g., Nelson, 1979; Auld, 1990]. For example, this holds for a frequency $f < 1$ GHz for a dimension of $X_{\max} = 1$ cm. Within the EQS approximation all magnetic effects are neglected. Then, the governing equations of piezoelectric waves are Newton–Cauchy's equation of motion, Poisson's equation, and the equation of deformation rate, which read for a volume V with the surface $S = \partial V$

$$\iiint_V \rho_{\mathrm{p0}}(\underline{\mathbf{R}})\dot{\underline{\mathbf{v}}}(\underline{\mathbf{R}},t)dV = \oiint_S \underline{\mathbf{n}}\cdot\underline{\underline{\mathbf{T}}}(\underline{\mathbf{R}},t)dS + \iiint_V \underline{\mathbf{f}}(\underline{\mathbf{R}},t)dV \tag{1}$$

$$\begin{aligned}\oiint_S \underline{\mathbf{n}}\cdot\underline{\underline{\boldsymbol{\varepsilon}}}^{\mathrm{S}}(\underline{\mathbf{R}})\cdot\boldsymbol{\nabla}\Phi(\underline{\mathbf{R}},t)dS &= \oiint_S \underline{\mathbf{n}}\cdot\underline{\underline{\mathbf{e}}}(\underline{\mathbf{R}}) : \mathrm{sym}\{\boldsymbol{\nabla}\underline{\mathbf{u}}(\underline{\mathbf{R}},t)\}dS \\ &\quad - \iiint_V \varrho(\underline{\mathbf{R}},t)dV - \iint_S \eta(\underline{\mathbf{R}},t)dS \end{aligned} \tag{2}$$

$$\begin{aligned}\iiint_V \underline{\underline{\underline{\mathbf{s}}}}^{\mathrm{E}}(\underline{\mathbf{R}}) : \dot{\underline{\underline{\mathbf{T}}}}(\underline{\mathbf{R}},t)dV &= \oiint_S \mathrm{sym}\{\underline{\mathbf{n}}\,\underline{\mathbf{v}}(\underline{\mathbf{R}},t)\}dS + \iiint_V \underline{\underline{\underline{\boldsymbol{\tau}}}}^{\mathrm{E}}(\underline{\mathbf{R}}) : \mathrm{sym}\{\boldsymbol{\nabla}\,\dot{\underline{\mathbf{v}}}(\underline{\mathbf{R}},t)\}dV \\ &\quad + \iiint_V \underline{\underline{\underline{\mathbf{d}}}}^{231}(\underline{\mathbf{R}})\cdot\boldsymbol{\nabla}\dot{\Phi}(\underline{\mathbf{R}},t)dV + \iiint_V \underline{\underline{\mathbf{h}}}(\underline{\mathbf{R}},t)dV \end{aligned} \tag{3}$$

with the volume force density vector $\underline{\mathbf{f}}$, particle displacement vector $\underline{\mathbf{u}}$, electric charge density ϱ, electric surface charge density η, source of deformation rate tensor $\underline{\underline{\mathbf{h}}}$, and the surface normal $\underline{\mathbf{n}}$. The dot indicates the first time derivate.

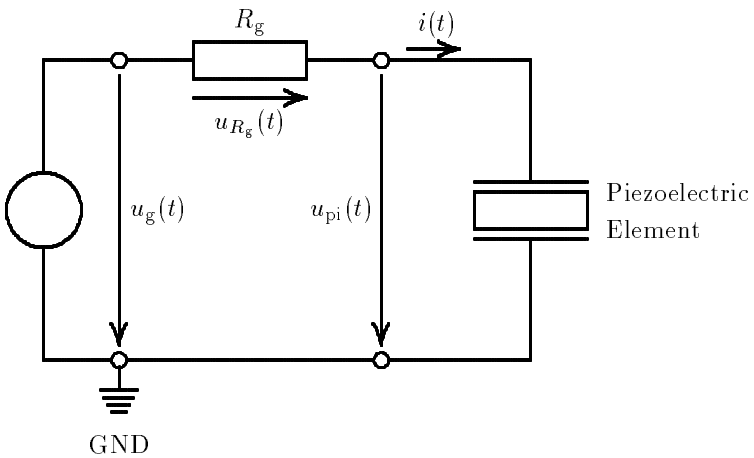

Figure 1. Equivalent electrical circuit.

The set of consistent matrix equations of the explicit elliptic–hyperbolic time domain algorithm PFIT [Marklein, 1997] is obtained by introducing a staggered grid system (G, $\widetilde{G}$) with the grid spacing Δx, applying the Finite Integration Technique (FIT) to Eq. (1)–(3), and discretizing time derivatives with finite difference formulas ($z = t/\Delta t$).

To include an external electrical load in the numerical scheme, which is in many cases an Ohmic resistance R_{g} (see Fig. 1), the current driven approach is combined with a network algorithm. A flowchart of the resulting algorithm is given in Fig. 2. SSOR and CG algorithms are implemented to solve Poisson's grid equation. In the following examples a CG algorithm with diagonal scaling (DCG) is applied.

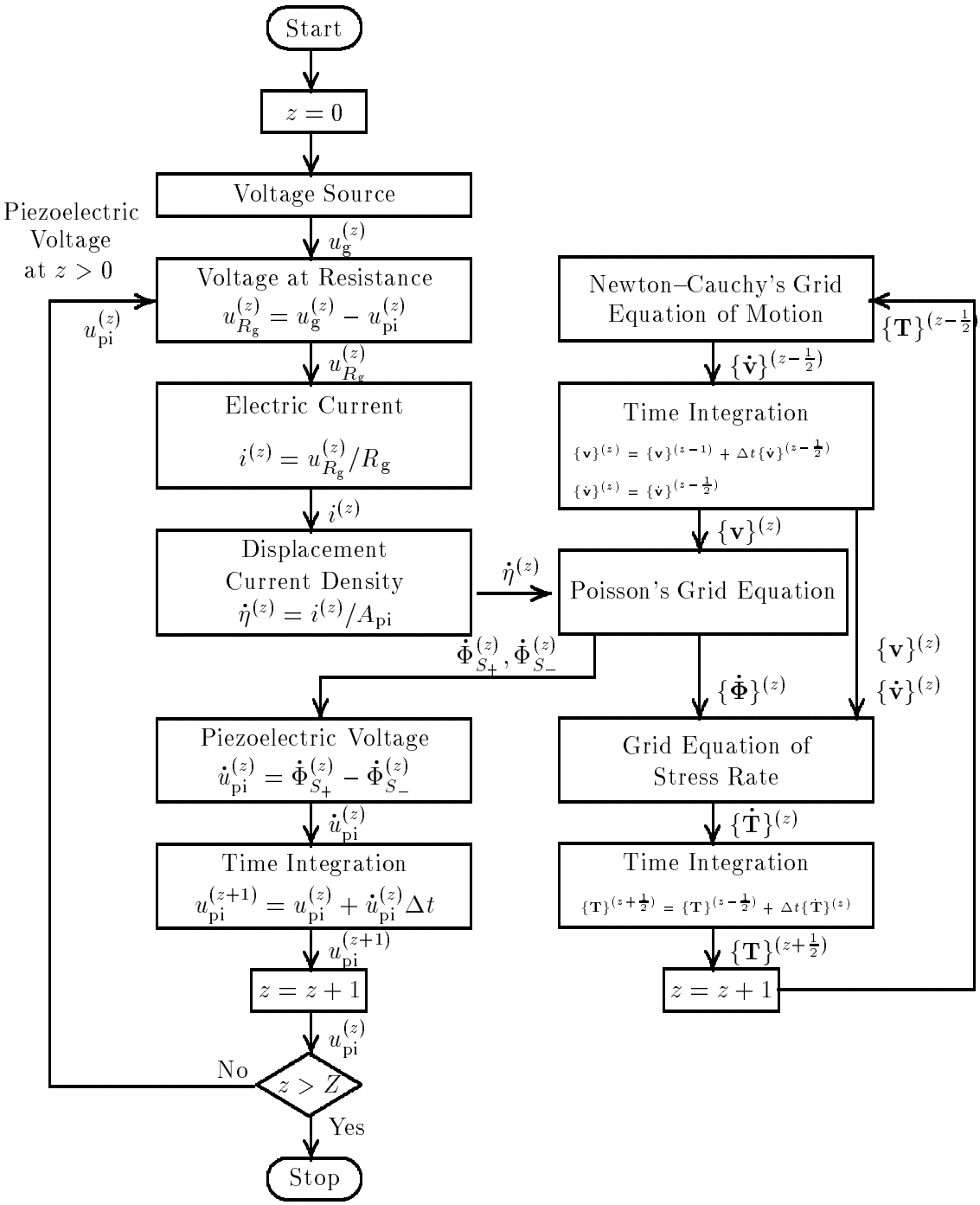

Figure 2. Combined network algorithm (left) and I–PFIT algorithm (right).

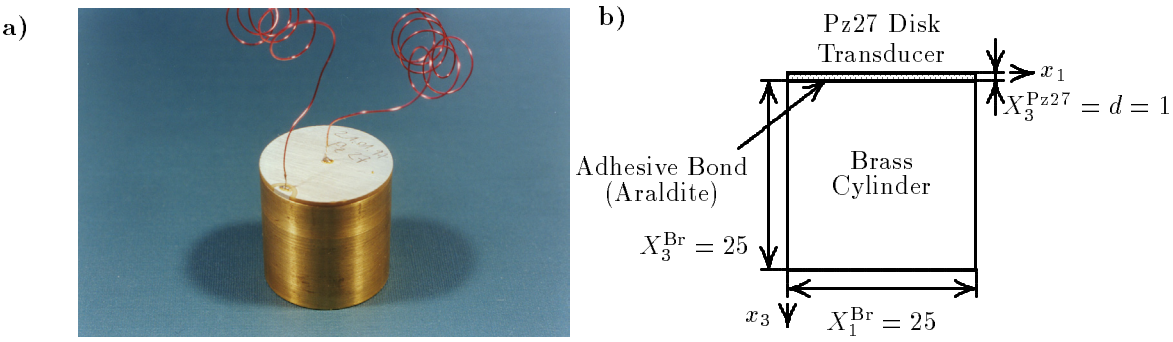

Figure 3. Ultrasonic piezoelectric Pz27 disk transducer on a brass cylinder: **a)** photograph and **b)** 2–D geometry for the 2–D PFIT modeling.

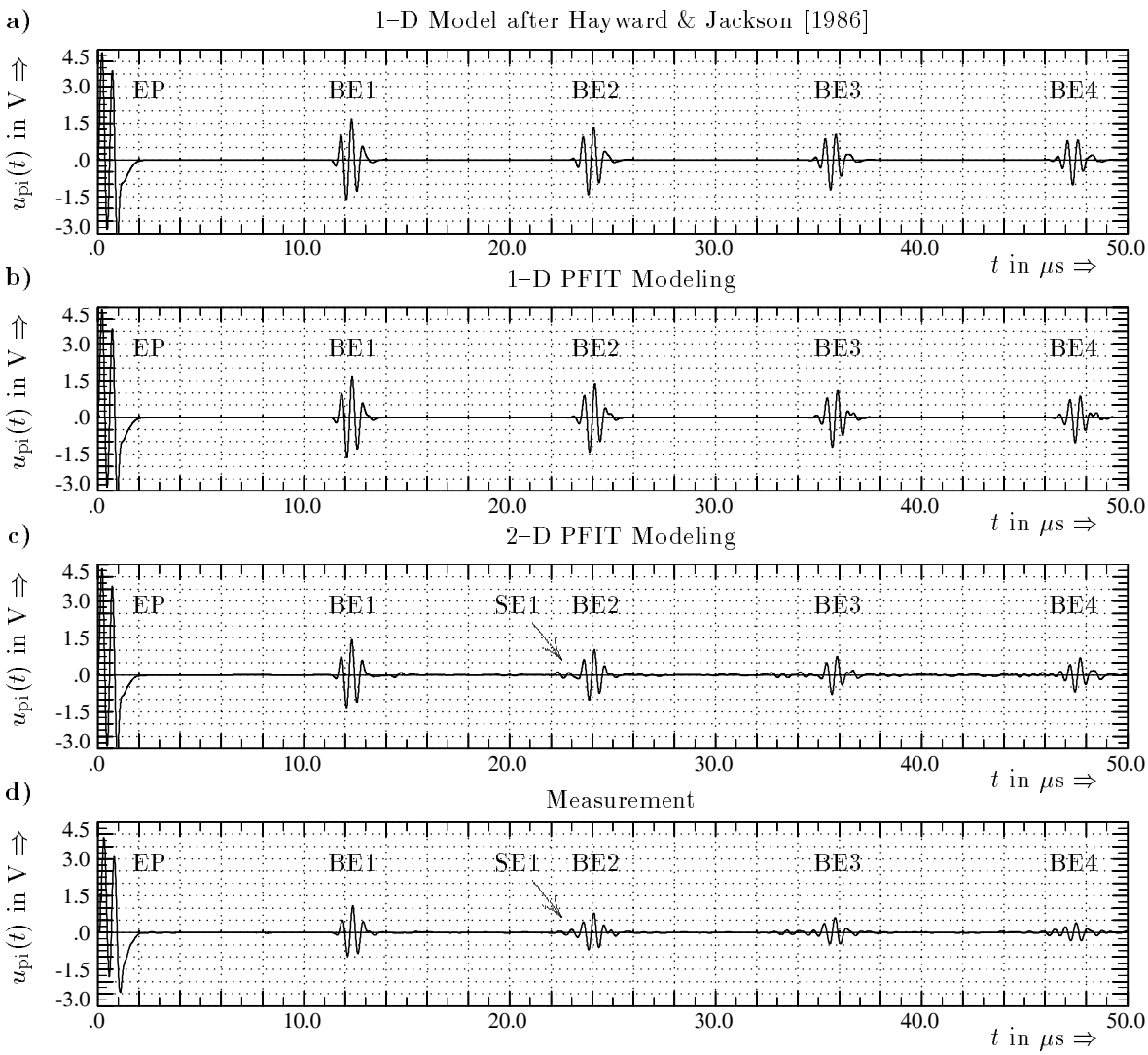

Figure 4. Ultrasonic piezoelectric Pz27 disk transducer on a brass cylinder: comparison **(a–d)** of the piezoelectric voltage u_{pi} at the Pz27 disk (A–scan) for $R_{\mathrm{g}} = 50\ \Omega$ and a sine pulse excitation with $u_0 = 10$ V, $n = 2$ cycles, and $f_{\mathrm{C}} = 2$ MHz. EP: excitation pulse; BEn: n–th backwall echo; SEn: n–th secondary echo.

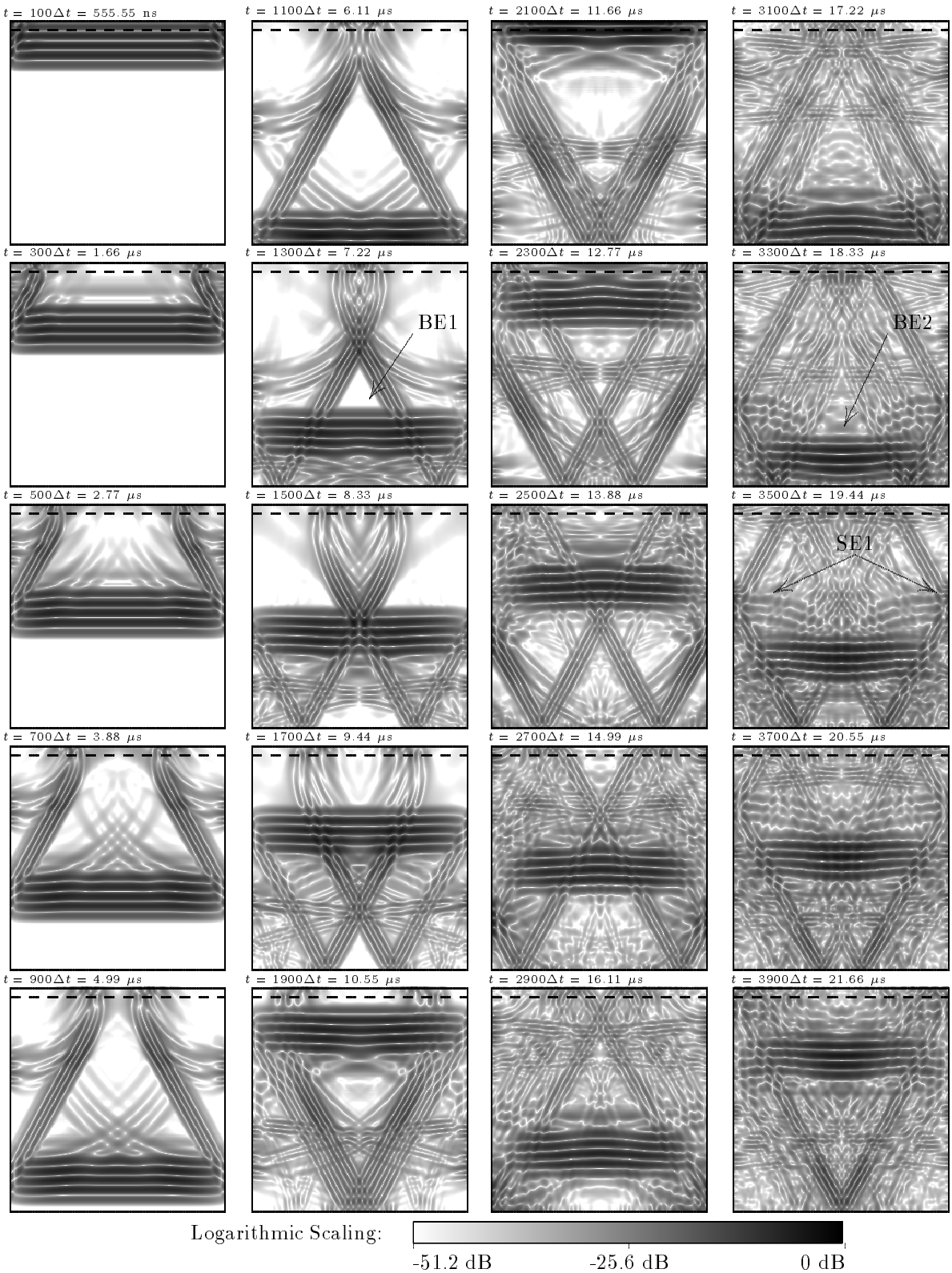

Figure 5. Ultrasonic piezoelectric Pz27 disk transducer on a brass cylinder: 2–D PFIT $|\{\widehat{\mathbf{v}}\}|$–snapshots. EP: excitation pulse; BEn: n–th backwall echo; SEn: n–th secondary echo.

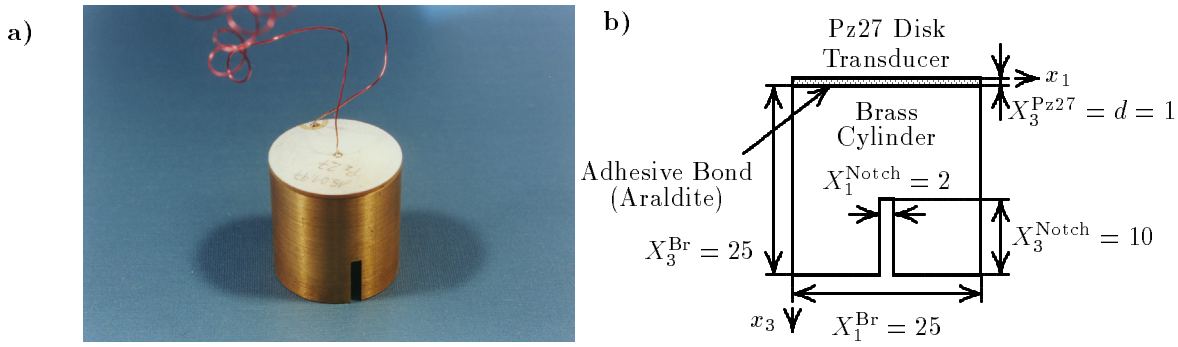

Figure 6. Ultrasonic piezoelectric Pz27 disk transducer on a brass cylinder with a backwall breaking notch: **a)** photograph and **b)** 2–D geometry for the 2–D PFIT modeling.

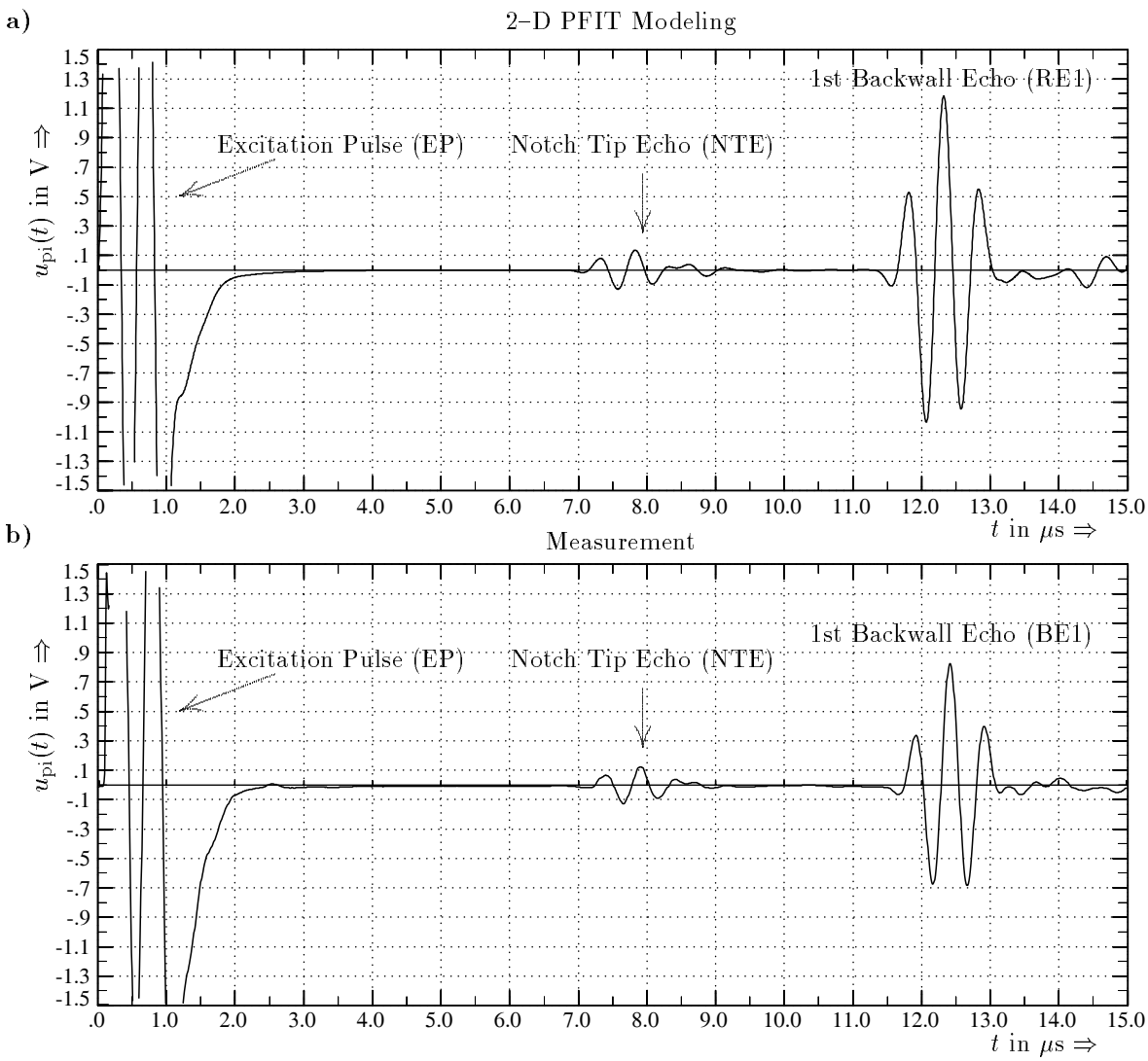

Figure 7. Ultrasonic piezoelectric Pz27 disk transducer on a brass cylinder with a backwall breaking notch: comparison between the modeled **(a)** and experimental **(b)** voltage u_{pi} at the Pz27 disk (A–scan) for $R_{\mathrm{g}} = 50\ \Omega$ and a sine pulse excitation with $u_0 = 10$ V, $n = 2$ cycles, and $f_{\mathrm{c}} = 2$ MHz. EP: excitation pulse; NTE: notch tip echo BE1: 1st backwall echo.

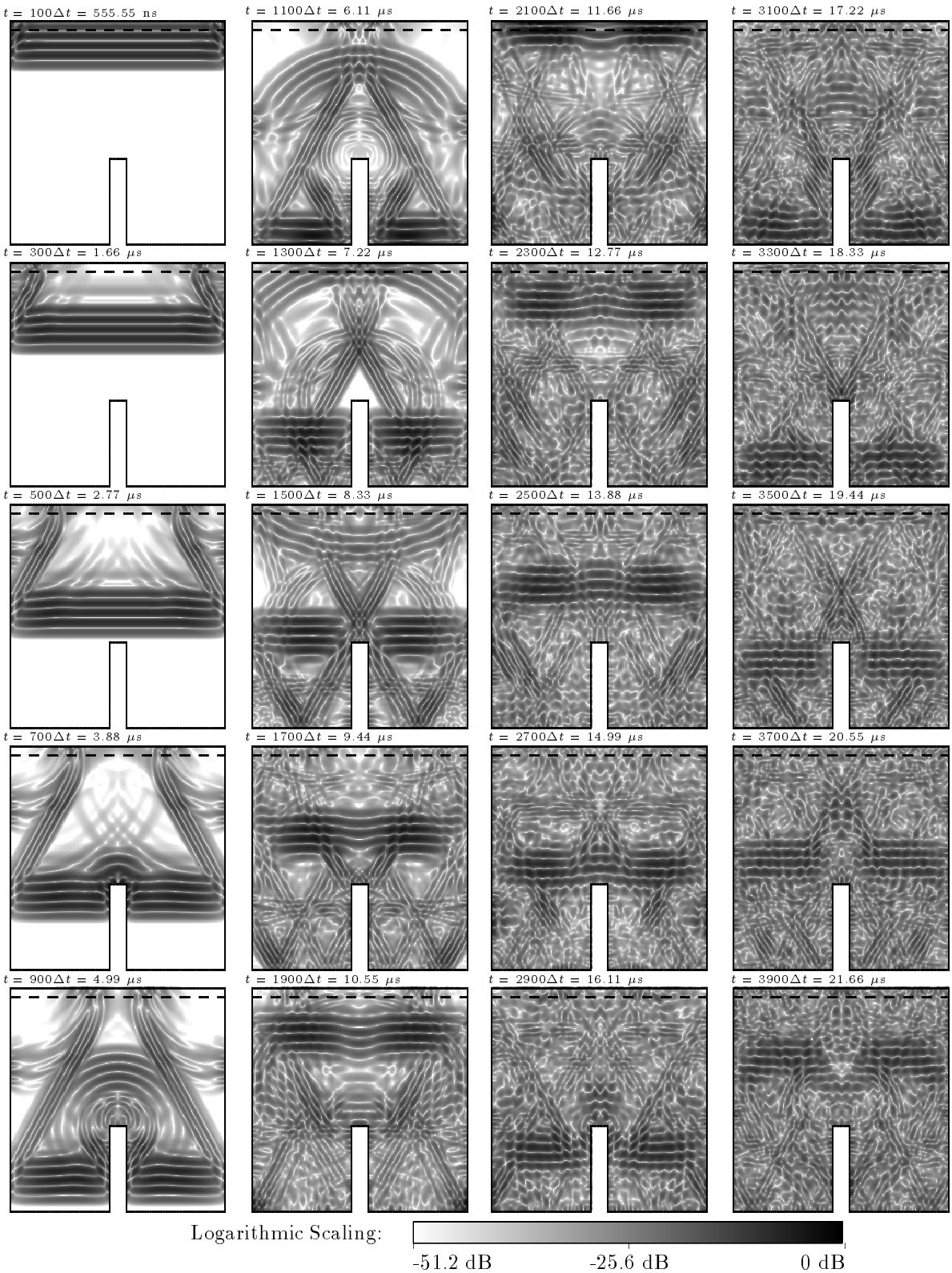

Figure 8. Ultrasonic piezoelectric Pz27 disk transducer on a brass cylinder: 2–D PFIT $|\{\widehat{\mathbf{v}}\}|$–snapshots. EP: excitation pulse; BEn: n–th backwall echo; SEn: n–th secondary echo.

NUMERICAL RESULTS AND VALIDATION WITH EXPERIMENTAL DATA

Fig. 3 shows a photograph of the first sample and the 2–D geometry for the 2–D PFIT modeling. The sample consists of a piezoelectric Pz27 disk transducer which is adhesively bonded on a brass cylinder. All materials are considered nondissipative. Fig. 4 shows a comparison of the voltage at the piezoelectric disk between the results of the 1–D model by Hayward & Jackson [1986], 1–D PFIT modeling, 2–D PFIT modeling, and the measurement. Especially the 2–D PFIT modeling gives an excellent agreement with the experimental results in respect to the amplitude decay of the backwall echos (BE) and the 1st secondary echo (SE1). The latter is missing in the 1–D modeling results, because this is a multidimensional effect. The snapshots shown in Fig. 5 explain the generation of each echo signal. A second sample is given in Fig. 6, it is the sample shown in Fig. 3 with a backwall breaking notch. A comparison between the modeled and experimental voltage is given in Fig. 7, which validates the numerical results. The dominant signals are the excitation pulse (EP), the notch tip echo (NTE), and the 1st backwall echo (BE1). Because of the 2–D modeling the experimental backwall echo (BE1) has a smaller amplitude. A sequence of 2–D PFIT $\{\hat{\mathbf{v}}\}$–snapshots is displayed in Fig. 8 showing the ultrasonic waves propagation and the generation of the notch tip echo (NTE) and the 1st backwall echo (BE1).

CONCLUSIONS

A novel numerical modeling tool called PFIT for the modeling of coupled piezoelectric and ultrasonic wave phenomena has been presented. The obtained results illustrating the power of PFIT and giving trust for further applications: to help to understand ultrasonic wave propagation, especially in complex materials and complex geometries, to optimize well–accepted NDT techniques, and/or to develop new and more efficient NDT techniques.

REFERENCES

1. Lerch, R., Simulation of Piezoelectric Devices by Two- and Three-Dimensional Finite Elements. *IEEE Trans. Ultrason. Ferroelect. Freq. Cont.*, Vol. 37, No. 2, May, pp. 233–247, 1990.
2. Roberts, M. J., *Numerical Modeling of Piezoelectric Transducer Arrays for Medical Imaging Systems.* Ph. D. Thesis, Worcester Polytechnic Institute, Worcester, Mass., USA, 1991.
3. Nelson, D. F., *"Electric, Optic, and Acoustic Interactions in Dielectrics,"* John Wiley & Sons, New York, USA, 1979.
4. Auld, B. A., *"Acoustic Fields and Waves in Solids,"* 2nd ed., R. E. Krieger Publishing Company, Malabar, Florida, USA, 1990.
5. Marklein, R., *"Numerical Methods for the Modeling of Acoustic, Electromagnetic, Elastic and Piezoelectric Wave Propagation Problems in the Time Domain Based on the Finite Integration Technique,"* Shaker Verlag, Aachen, Germany, 1997. (in German)
6. Hayward, G., M. N. Jackson, A Lattice Model of the Thickness–Mode Piezoelectric Transducer. *IEEE Trans. Ultrason. Ferroelect. Freq. Cont.*, Vol. 33, No. 1, pp. 41–50, 1986.